Tellus (2000), 52A, 440–454
Printed in UK. All rights reserved

TELLUS
ISSN 0280–6495

Extremal climatic states simulated by a 2-dimensional model

Part II: Different climatic scenarios

By TONI PUJOL*[1,2] and JOSEP ENRIC LLEBOT[2], [1]*Dept. de Física, Facultat de Ciències, Universitat de Girona, 17071 Girona, Catalonia, Spain;* [2]*Dept. de Física, Facultat de Ciències, Universitat Autònoma de Barcelona, 08193 Bellaterra, Catalonia, Spain*

(Manuscript received 7 May 1999; in final form 28 January 2000)

ABSTRACT

Different climatic simulations have been obtained by using a 2-Dim horizontal energy balance model (EBM), which has been constrained to satisfy several extremal principles on dissipation and convection. Moreover, 2 different versions of the model with fixed and variable cloud-cover have been used. The assumption of an extremal type of behaviour for the climatic system can acquire additional support depending on the similarities found with measured data for past conditions as well as with usual projections for possible future scenarios.

1. Introduction

The purpose of this paper is to investigate the predictive capability of some extremal principles which can be applied to the climatic system. In analogy with thermodynamics, these principles are related to several contributions of entropy production (i.e., dissipation) as well as to the convection of the system. In Part I, the main characteristics of these hypotheses have been obtained, which can be summarized as follows: (1) the hypothesis of maximum convection governs the cloud-cover reached by the system. Therefore, climatic simulations where both convective and dissipative hypotheses are applied, become similar and independent on the dissipation hypothesis which has been assumed. (2) If the cloud-cover has been fixed, the temperature distribution of the climate at the maximum state in total entropy production tends to be latitudinally homogeneous, whilst the state at the maximum state in material entropy production becomes similar to that found with a variable cloud-cover. (3) The principle of minimum radiative entropy production, based on one of Planck's results (Planck, 1913), depends on the structure and dimension of the model. (4) If the cloud-cover is a free-variable, the ice-albedo feedback causes smaller changes in cloud-cover and similar ones in temperature than simulations carried out with a constant surface albedo, and implies greater variations in temperature for a fixed cloud version. (5) The climatic sensitivity is greater for the variable cloud model (where both maximum convection and dissipation hypotheses are applied) than for the fixed one (extremal principles only related to dissipation).

However, although in Part I we pointed out the feasible application of the principle of maximum material entropy production based on the results obtained for current conditions, further analyses are required due to no theoretical demonstrations were obtained. Here, we show a detailed analysis of different climatic scenarios simulated by means of applying extremal principles, from which similarities with measured data and climatic projections

* Corresponding author.
e-mail: caaps@fc.udg.es

obtained by usual climatic models can provide additional support for the application of the extremal principles to the climate.

The structure of the paper is as follows: in Section 2 we briefly describe the model used. Section 3 is focused on pre-industrial–present results whereas those related to possible future scenarios are indicated in Section 4. In Section 5 the role of the ice-albedo feedback within the model used has been analyzed and, finally, we conclude in Section 6 with a discussion and a comparison of the results obtained.

2. Model

The 2-Dim horizontal model was described in Part I. Here, its main characteristics are summarized: (1) it is formed by 32×32 boxes of equal surface area which cover the entire globe; (2) each box is subdivided into atmospheric and oceanic regions; (3) the only free variables are temperature, convective fluxes, advective fluxes and cloud-cover, which otherwise can be fixed; (4) the method of solution of the model uses two energy balance equations for each box plus two extremal hypotheses, which are related to convection and dissipation (only one if the cloud-cover has been fixed); (5) dissipation hypotheses have been applied through extremizing the material (advection plus convection), radiative, advective or total (i.e., radiative plus material) parts of entropy production.

On the other hand, the short-wave parameters used in the model are: atmospheric absorption α_a, absorption by water drops in clouds α_c, surface albedo α_s, cloud albedo ω_c and clear-sky albedo ω_g. The long-wave parameters are: atmospheric m_a, cloud top m_c and cloud base n_c emissivities related to surface temperature, and the fraction of surface radiation which is directly lost to space m_g. For comparison purposes with 1-Dim versions of this model, all the long-wave parameters for current conditions have been chosen as constant values both in latitude as in longitude. The short-wave parameters are only a function of latitude, being independent on longitude, excepting the surface albedo that is the only parameter in the 2-Dim model which varies in both latitude and longitude.

3. Pre-industrial conditions

The pre-industrial state has been chosen as that equivalent to the climatic conditions obtained in the year 1750. Changes in greenhouse gases as well as aerosol concentration have been introduced by varying both long- and short-wave parameters used in the 2-Dim model. Thus, the effect of anthropogenic greenhouse gases over the pre-industrial–present period has been assumed to change the surface emissivity m_g (Grassl, 1981). For the pre-industrial–present period, a reduction in m_g equal to -0.008 has been used, which causes a radiative forcing ≈ 2.2 W m^{-2} (within the range of estimated values proposed by the IPCC 1995). Moreover, following Grassl (1981), the variation in m_c corresponds to 48% of the change in m_g. Also, the variation in both emissivities has been taken as latitudinal dependent, with the aim of simulating the overlap between both CO_2 and water vapour absorption bands. In particular, the difference between two consecutive boxes is equal to 1.6% of the global mean variation, increasing towards the pole (Grassl, 1981).

In contrast, the pre-industrial–present variation in aerosols has been assumed to be longitudinal dependent, following Haywood and Ramaswamy (1998). Thus, the hemispheric distribution of the radiative forcing due to the direct effect of aerosols equals NH : SH = 1.40 : 0.24. With the aim of giving a simple evaluation of the indirect effect, a similar distribution to that due to the direct effect has been used with a hemispheric ratio for the radiative forcing as NH : SH = 0.70 : 0.24, being half of that considered for the direct effect (IPCC, 1995). From the sensitivity analysis carried out in Part I, the direct effect of aerosols causes a variation in clear-sky albedo ω_g equal to $\Delta\omega_g = 1.4 \times 10^{-3}$, which has been obtained by assuming a long-wave radiative forcing at the top of the atmosphere TOA (ΔH_{LT}) as -0.5 Wm^{-2}. Finally, the indirect effect of aerosols modifies the albedo for cloudy regions ω_c, which following the sensitivity analysis varies $\Delta\omega_c = 1.5 \times 10^{-3}$ for a -0.4 W m^{-2} indirect radiative forcing.

3.1. Variable cloud-cover

For the variable cloud model, both maximum convection and maximum dissipation hypotheses have been used. The convective principle governs the cloud-cover reached by the system and, therefore, the application of different dissipation principles produces similar results.

3.1.1. Globally-averaged results. Globally-averaged differences of temperature T, cloud-cover ϑ, long-wave radiation at TOA H_{LT} and planetary albedo α_p for the pre-industrial–present period are shown in Table 1, where the maximum rate of material entropy production σ_m has been applied (first four numerical columns). These results are compared with those deduced at the maximum rate of total entropy production σ_t, also shown in Table 1 (last four columns). Both cases have been obtained with the ice-albedo feedback. In Table 1, the effect of both greenhouse gases and aerosols have been analyzed separately. Thus, a climatic simulation with a radiative forcing ≈ -0.5 W m^{-2} at TOA, only due to the direct effect of aerosols, has been obtained. Due to the uncertainties of the indirect effect (Charlson et al., 1992; Langner et al., 1992), two different values equivalent to -0.4 and -0.8 W m^{-2} radiative forcing at TOA have been applied. Finally, a greenhouse-gas only climatic simulation has been obtained, which includes a radiative forcing at TOA equivalent to that assumed for the pre-industrial–present period for both greenhouse gases and aerosols.

The global contribution of both greenhouse gases and the direct effect of aerosols implies a globally-averaged warming ≈ 1.1°C and a reduction in globally-averaged cloud fraction ≈ 2.2% at the maximum state in σ_m and ≈ 1.6% at the maximum state in σ_t, for the pre-industrial–present period. In comparison, Taylor and Penner (1994) have found a globally-averaged warming of 2.1°C only due to greenhouse gases, with a reduction in 1.5% of the cloud-cover obtained by applying a global climate model (GCM) in conjunction with a tropospheric chemistry model and, for example, Mitchell et al. (1995) have obtained a warming ≈ 0.7°C only due to greenhouse gases, whilst ≈ 0.5°C is obtained when the direct effect of aerosols is introduced in a GCM.

The assumption of an indirect effect of aerosols equivalent to a radiative forcing at TOA ≈ -0.8 W m^{-2} from pre-industrial conditions (Taylor and Penner, 1994), reduces the globally-averaged warming to 0.9°C, with a variation in globally-averaged cloud fraction ≈ -0.5% (i.e., decrease for the pre-industrial–present period) and 0.2% (i.e., increase for the pre-industrial–present period) at the states of maximum material and total entropy production respectively.

3.1.2. Climatic sensitivity. From Table 1, the climatic sensitivity λ_T (the ratio of global-average temperature response to global-average forcing; $\lambda_T = \Delta T/\Delta H_{LT}$) differs according to the effect considered as can be seen in Table 2. Furthermore, in Table 2 the climatic sensitivity of cloud-cover λ_ϑ (i.e., the ratio of global-average cloud response to global-average forcing; $\lambda_\vartheta = \Delta\vartheta/\Delta H_{LT}$) is also shown. The sensitivity of the climatic system simu-

Table 1. *Globally-averaged pre-industrial–present changes in T temperature, ϑ cloud-cover, LE + H latent plus sensible heat fluxes, H_{LT} long-wave radiation fluxes at top of the atmosphere (TOA) and α_p planetary albedo, with variable cloud-cover*

	Climate at the maximum state in σ_m				Climate at the maximum state in σ_t			
Effect	ΔT (°C)	$\Delta\vartheta$ (%)	ΔH_{LT} (W m^{-2})	$\Delta\alpha_p$ (×100)	ΔT (°C)	$\Delta\vartheta$ (%)	ΔH_{LT} (W m^{-2})	$\Delta\alpha_p$ (×100)
greenhouse gases[1]	1.29	−2.68	2.19	−0.65	1.32	−2.12	2.17	−0.57
[2]	0.53	−1.10	0.90	−0.27	0.55	−0.87	0.89	−0.23
aerosols direct effect[3]	−0.15	0.47	−0.52	0.15	−0.15	0.50	−0.52	0.16
aerosols indirect effect[4]	−0.12	0.89	−0.41	0.12	−0.11	0.94	−0.41	0.13
[5]	−0.23	1.72	−0.82	0.25	−0.23	1.81	−0.82	0.26

[1]Assuming a global radiative forcing ≈ 2.2 W m^{-2} for the pre-industrial–present period.
[2]Assuming a global radiative forcing (greenhouse gases + aerosols) only produced by greenhouse gases.
[3]Direct effect of aerosols assuming variations in clear-sky albedo.
[4]Slight indirect effect of aerosols.
[5]Moderate indirect effect of aerosols.

Table 2. *Climatic sensitivity $\lambda_T (KW^{-1} m^2)$ and λ_ϑ (% $W^{-1} m^2$) for greenhouse gases and aerosols*

		Greenhouse gases		Aerosols		
		[1]	[2]	direct[3]	indirect[4]	indirect[5]
λ_T	σ_p	0.59	0.60	0.29	0.28	0.28
	σ_m	0.59	0.59	0.29	0.28	0.28
	σ_t	0.61	0.61	0.29	0.28	0.28
λ_ϑ	σ_p	−1.16	−1.16	−0.94	−2.22	−2.15
	σ_m	−1.22	−1.22	−0.90	−2.17	−2.09
	σ_t	−0.98	−0.97	−0.96	−2.27	−2.20

[1] Assuming a global radiative forcing ≈ 2.2 W m^{-2} for the pre-industrial–present period.
[2] Assuming a global radiative forcing (greenhouse gases + aerosols) only produced by greenhouse gases.
[3] Direct effect of aerosols assuming variations in clear-sky albedo.
[4] Slight indirect effect of aerosols.
[5] Moderate indirect effect of aerosols.

lated by the model at the maximum state of material entropy production σ_m for a greenhouse gas-only scenario becomes similar to that projected by the "best estimation" of the IPCC, being $\lambda_T \approx 0.59$ KW^{-1} m^2 (IPCC, 1995). A slight increase has been obtained at the maximum state of total entropy production σ_t, which, however, is considerably lower than recent values obtained by GCMs (e.g., $\lambda_T \approx 1.0$ KW^{-1} m^2; Hewitt and Mitchell, 1997). Both direct and indirect effects of aerosols have a similar value of climatic sensitivity λ_T, being lower than that obtained for the greenhouse gases. In addition, the indirect effect of aerosols influences the cloud-cover more than changes in greenhouse gases or the direct effect of aerosols.

3.1.3. Zonally-averaged results. Zonally-averaged distributions of temperature and cloud-cover for the pre-industrial–present period permit us to observe the intense localized cooling effect of aerosols in the simple energy balance model (EBM) analyzed. Zonally-averaged changes in surface temperature for the pre-industrial–present period at the maximum state of material entropy production σ_m are shown in Fig. 1. The warming due to the increase in greenhouse gases varies slightly in latitude, being less at equatorial regions and greater at mid and high latitudes. The effect of aerosols is mainly located at mid-latitudes in the Northern Hemisphere, following the spatial distribution shown by Haywood and Ramaswamy (1998). However, this result does not agree with simulations obtained by GCMs. Thus, for example, Reader and Boer (1998) have found that both greenhouse gas and aerosol patterns of changes in temperature are similar. These notable differences are not a consequence of the extremal principle applied but to the simple thermodynamic 2-Dim model used in this paper, from which the climatic dynamics has not been deduced explicitly. Therefore, the system tends to respond locally. However, it does not invalidate our calculations

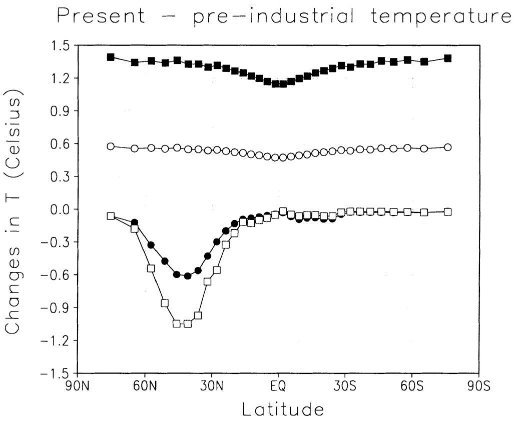

Fig. 1. Pre-industrial–present zonally-averaged changes in temperature. Simulations to the maximum rate of σ_m. Closed squares = greenhouse gases, closed circles = direct effect of aerosols, open squares = indirect effect of aerosols (moderate), open circles = equivalent greenhouse gases (i.e., the effect of greenhouse gases plus aerosols for the pre-industrial–present period only assumed to correspond to greenhouse gases).

at all, since our purposes are focused on finding the projected states obtained by applying several additional extremal constraints to a simple picture of the climate, taking the intrinsic limitations of the model into account. Thus, although one is tempted to compare the climatic simulations with results based on similar EBMs, the comparison must be made with GCMs due to these models include the most important processes that govern the climate system. In fact, the assumption of an extremal hypothesis is made for reducing the number of parameterizations used in usual EBMs, and is expected to produce a better simulation of the real climatic behaviour. Thus the basic idea is that a general principle could be applied in different climatic scenarios where some of the relationships assumed in many EBMs are not necessarily valid (e.g., the diffusive hypothesis with constant planetary "diffusivity"). Therefore, the comparison of the results with simulated data has been based on numerical output from GCMs, taking the limitations of the present model into account.

Thus the results show as the local increase of aerosols causes an increase in cloud-cover, which is opposite to the effect of greenhouse gases, as can be seen from Fig. 2. Then, for the pre-industrial–present period the model simulates regions with negative and positive changes in zonally-averaged cloud fraction, when both greenhouse gases and aerosols effects have been taken into account.

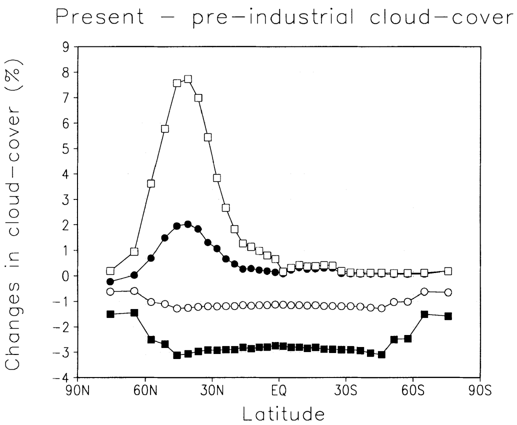

Fig. 2. Pre-industrial–present zonally-averaged changes in cloud-cover. Simulations to the maximum rate of σ_m. Closed squares = greenhouse gases, closed circles = direct effect of aerosols, open squares = indirect effect of aerosols (moderate), open circles = equivalent greenhouse gases (i.e., the effect of greenhouse gases plus aerosols for the pre-industrial–present period only assumed to correspond to greenhouse gases).

3.2. *Fixed cloud-cover*

The fixed cloud model only considers three independent variables; temperature T, convective heat fluxes $LE + H$ and advective heat fluxes X. In this case, the additional constraint corresponds to the maximum dissipation hypothesis, which is applied to the rate of total σ_t, material σ_m or advective σ_p entropy production. (Simulations at the minimum state in radiative entropy production σ_r have not been carried out due to the unrealistic distribution produced for this hypothesis seen in Part I.) The cloud-cover has been fixed and follows that obtained for current conditions in the cloud variable model. Thus cloud-cover distributions of total, material and advective entropy production do not coincide. The main differences are observed at high latitudes where the cloud-cover at the maximum state in material entropy production σ_m reaches high values, in contrast to both distributions found for σ_t and σ_p.

3.2.1. Globally-averaged results. Changes in long- as well as in short-wave parameters related to the pre-industrial–present period are those described in Subsection 3.1. Globally-averaged changes in surface temperature T, long-wave radiation at TOA H_{LT}, and planetary albedo α_p are shown in Table 3 for both maximum states in σ_m and in σ_t, including the ice-albedo feedback. The model is applied in stationary conditions and, therefore, long-wave changes at TOA are equal to short-wave changes at TOA. For a model with fixed cloud-cover, changes in long-wave parameters, such as those caused by the effect of greenhouse gases, do not modify the short-wave radiation unless the surface albedo is a function of temperature. Therefore, climatic simulations of changes in greenhouse gases without the ice-albedo feedback and with a fixed cloud-cover do not modify both radiative forcing at TOA and planetary albedo. Moreover, the radiative changes at TOA due to greenhouse gases when the ice-albedo feedback is introduced, become very small. Here, we point out that the expected real changes at TOA due to variations in the sea ice-snow line are considerable. Such a low variation in H_{LT}

Table 3. *Globally-averaged pre-industrial–present changes in T temperature, LE + H latent plus sensible heat fluxes, H_{LT} long-wave radiation fluxes at top of the atmosphere and α_p planetary albedo, with a fixed cloud-cover*

	Climate at the maximum state in σ_m			Climate at the maximum state in σ_t		
Effect	ΔT (°C)	ΔH_{LT} ($W m^{-2}$)	$\Delta\alpha_p$ ($\times 100$)	ΔT (°C)	ΔH_{LT} ($W m^{-2}$)	$\Delta\alpha_p$ ($\times 100$)
greenhouse gases[1]	0.69	0.06	−0.04	0.72	0.08	−0.05
[2]	0.28	0.03	−0.01	0.29	0.03	−0.02
aerosols direct effect[3]	−0.21	−0.65	0.20	−0.21	−0.65	0.20
aerosols indirect effect[4]	−0.14	−0.45	0.13	−0.14	−0.45	0.14
[5]	−0.28	−0.89	0.27	−0.29	−0.90	0.28

[1]Assuming a global radiative forcing ≈ 2.2 W m^{-2} for the pre-industrial–present period.
[2]Assuming a global radiative forcing (greenhouse gases + aerosols) only produced by greenhouse gases.
[3]Direct effect of aerosols assuming variations in clear-sky albedo.
[4]Slight indirect effect of aerosols.
[5]Moderate indirect effect of aerosols.

found when changing the surface albedo is a consequence of the simple model used, where the planetary albedo α_p is mainly influenced by cloudy ω_c and clear-sky albedos ω_g, being less intense the effect of surface albedo α_s.

In contrast, changes in short-wave parameters, such as those produced by the effect of aerosols, are similar to those obtained for a variable cloud model. Thus the globally-averaged greenhouse-gas only warming becomes similar to that obtained by Mitchell et al. (1995) in a GCM, which is ≈ 0.7°C. When the direct effect of aerosols is included, globally-averaged changes in temperature for the pre-industrial–present period are ≈ 0.5°C. This warming is even more reduced if we assume a moderate indirect effect of greenhouse gases (radiative forcing at TOA = -0.8 W m^{-2}), being ≈ 0.2°C. Furthermore, cases involving aerosols are associated with negative radiative forcings at TOA from the pre-industrial state, because changes in long-wave parameters only cause small variations in the net balance at TOA as a consequence of the ice-albedo feedback.

On the other hand, simulations with and without ice-albedo feedback are similar, and follow those shown in Table 3. Moreover, results assuming states at maximum advective entropy production behaves like those shown in Table 3.

3.2.2. Climatic sensitivity. In comparison with Table 1, the warming due to the greenhouse gas-only effect has been reduced considerably. The effect of aerosols, however, remains similar. In this case, the climatic sensitivity of greenhouse gases cannot be obtained due to the reduced variation of long-wave radiation at TOA. The climatic sensitivity for both direct and indirect effects of aerosols becomes similar, being $\lambda_T \approx 0.32$ KW^{-1} m^2, which is a value slightly greater than that obtained for a variable cloud model.

3.2.3. Zonally-averaged results. Zonally-averaged results for the pre-industrial–present period behave similar to those observed in Fig. 1, taking the reduced warming due to the greenhouse gas effect into account.

4. Possible future scenarios

Possible future scenarios simulated by the model have been obtained for different levels of the CO_2 equivalent concentration. The effect of greenhouse gases has been introduced by varying long-wave parameters, as has been used in the preceding section. Thus, the parameter m_g is reduced by -0.0165 for simulating a state doubling the current CO_2 equivalent concentration. Moreover, m_c is 48% of the variation in m_g. Both changes in the parameters increase towards the poles with a difference between two consecutive boxes equal to 1.6% of the mean variation in the parameter itself. This behaviour can be seen to represent the overlap between CO_2 and water vapour absorption bands (Grassl, 1981).

4.1. Variable cloud-cover

In this case, both hypotheses of maximum convection and dissipation have been applied.

4.1.1. Globally-averaged results. Globally-averaged changes in surface temperature T, cloud-cover ϑ, long-wave radiation at TOA H_{LT} and planetary albedo α_p are shown in Table 4 for different levels of CO_2 concentration, being simulations that include the ice-albedo feedback. Changes in the climate at maximum states in both material σ_m and advective σ_p entropy production are similar. In contrast, changes in temperature for climates at the maximum in σ_t become greater, whereas changes in cloud-cover are considerably smaller. Moreover, the introduction of the ice-albedo feedback mainly reduces those changes in cloud-cover but slightly those in temperature. This type of behaviour is due to the effect of the convective hypothesis, which dominates the value reached for the cloud fraction. Thus, when the ice-albedo feedback is taken into account, an increase in greenhouse gases reduces the surface albedo, which implies an increase in convective fluxes compared to that obtained with a constant surface albedo. Therefore, the reduction in cloud-cover due to the increase in greenhouse gases is less pronounced if the ice-albedo feedback has been used.

Table 4. *Globally-averaged changes in T temperature, ϑ cloud-cover, $LE + H$ latent plus sensible heat fluxes, H_{LT} long-wave radiation fluxes at the top of the atmosphere and α_p planetary albedo for different levels of CO_2; case with ice-albedo feedback and with variable cloud-cover*

Case ($\times CO_2$)	ΔT (°C)	$\Delta\vartheta$ (%)	ΔH_{LT} ($W\ m^{-2}$)	$\Delta\alpha_p$ ($\times 100$)
		maximizing σ_p		
0.5	−2.52	4.93	−4.28	1.23
1.5	1.55	−2.98	2.55	−0.74
2	2.68	−5.21	4.38	−1.28
3	4.33	−8.32	6.99	−2.05
4	5.54	−10.58	8.88	−2.61
		maximizing σ_m		
0.5	−2.52	5.29	−4.32	1.28
1.5	1.55	−3.14	2.57	−0.77
2	2.69	−5.41	4.42	−1.32
3	4.34	−8.73	7.04	−2.10
4	5.55	−11.08	8.94	−2.67
		maximizing σ_t		
0.5	−2.57	4.21	−4.28	1.13
1.5	1.59	−2.52	2.56	−0.68
2	2.76	−4.41	4.39	−1.16
3	4.45	−7.21	7.03	−1.89
4	5.70	−9.10	8.93	−2.38

The globally-averaged warming obtained at the $2CO_2$ doubling point agrees with the "best estimate" projection of the IPCC (1995), this being ≈ 2.7°C for the 3 expressions extremized. It also agrees with the estimation of the warming of equilibrium response to a doubling of CO_2 by an EBM (≈ 2.8°C) with a negative feedback from cloud radiative properties (Senior and Mitchell, 1993). Moreover, this value is ranged between those typical values obtained through using GCMs (≈ 3.0°C) and EBMs (≈ 2.5°C; from Kacholia and Reck, 1997). However, some differences appear in the variation of cloud-cover. Thus, reductions ≈ 5.4% and 5.2% have been obtained for the maximum states of material σ_m and advective σ_p entropy production during the present–$2CO_2$ period respectively, whereas the maximum state of total entropy production σ_t only projects a reduction ≈ 4.4%. A quadrupling of the CO_2 content only produces a globally-averaged warming ≈ 5.5°C, but a reduction in cloud-cover ≈ 10%. Thus globally-averaged changes in temperature and cloud-cover for the present–$4CO_2$ period are nearly two times those obtained for the present–$2CO_2$ period.

4.1.2. Zonally-averaged results. Although globally-averaged values are similar, zonally-averaged distributions become substantially different in relation to the expression extremized. In Fig. 3, zonally-averaged changes in temperature corresponding to the present–$2CO_2$ period are shown for three different extremal principles. Changes for the states of maximum total entropy production σ_t show a great variation in latitude. At the pole-boxes, the warming becomes a maximum reaching ≈ 4.2°C, whereas at equatorial regions, it is only 2.1°C. On the other hand, the zonally-averaged distribution of the warming foreseen at the maximum rate of material entropy production σ_m is similar to that obtained by maximizing the advect-

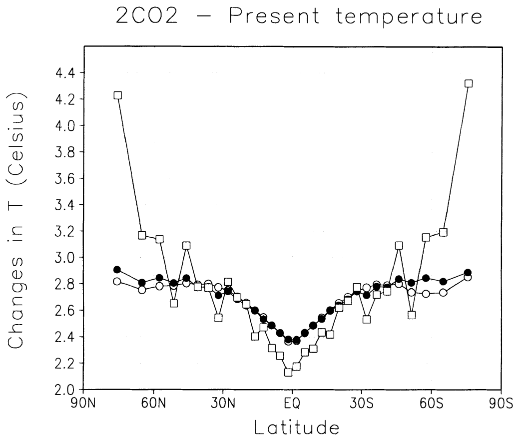

Fig. 3. Zonally-averaged changes in temperature for the present–$2CO_2$ case. Open circle = maximum state in σ_p, closed circle = maximum state in σ_m and open square = maximum state in σ_t.

ive part of material entropy production σ_p only. For both cases, a minimum warming has been found in equatorial regions, which is 2.4°C. The warming increases at the pole-boxes, reaching more than 2.8°C, being maximum at the Southern Hemisphere.

Zonally-averaged changes in cloud-cover for the present–$2CO_2$ point are shown in Fig. 4 for the different expressions extremized. Changes in

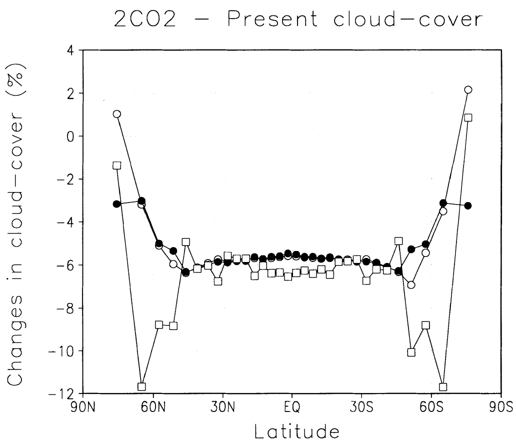

Fig. 4. Zonally-averaged changes in cloud-cover for the present–$2CO_2$ case. Open circle = maximum state in σ_p, closed circle = maximum state in σ_m and open square = maximum state in σ_t.

cloud-fraction practically do not vary in latitude for those regions where the ice-albedo feedback does not intervene. At high latitudes, the reduction in cloud-cover due to the increase in greenhouse gases is less important for the maximum states in σ_p and σ_m. Furthermore, the variation for the maximum state in advective entropy production σ_p is positive at high latitudes, as well as is found for the σ_t case at the Southern Hemisphere. In these cases, the regions with the greatest warming coincide with those where the cloud-cover increases.

4.1.3. Horizontal distribution. Changes in surface temperature for the present–$2CO_2$ period are also shown in Fig. 5 in a 2-Dim horizontal distribution (when including the ice-albedo feedback). Fig. 5a has been obtained through maximizing the advective entropy production σ_p. The region of greatest warming has been observed at the southern pole, although mid-latitudes reach a similar warming. Fig. 5b represents the warming at the $2CO_2$ point by maximizing the material entropy production σ_m. In this case the regions with maximum warmings are those located at the poles, reaching more than 2.9°C. Finally, Fig. 5c shows the distribution of changes in temperature obtained at the maximum state in total entropy production σ_t for the present–$2CO_2$ case. Notable differences are observed in comparison with the above results. Thus, the minimum warming appears in oceans at equatorial latitudes. In contrast, the surface temperature in desert regions increases $\approx$3.2°C (Sahara, Namibia, Australia, etc.). The regions with greater warming are, however, those located at high latitudes. For example, the surface temperature increases more than 4.2°C at the southern pole.

Cloud-cover changes have been also obtained in a 2-Dim distribution. Fig. 6a shows the variation in cloud-fraction for the present–$2CO_2$ case by applying the hypothesis of maximum advective entropy production σ_p. In this case, the cloud fraction increases at high latitudes.

Fig. 6b shows the variation in cloud-cover for the same period but corresponding to the maximum state in material entropy production σ_m. In this case, however, the cloud-cover mainly decreases in desert regions and evolves with small changes in the pole-boxes. The simulation at the maximum state in total entropy production σ_t

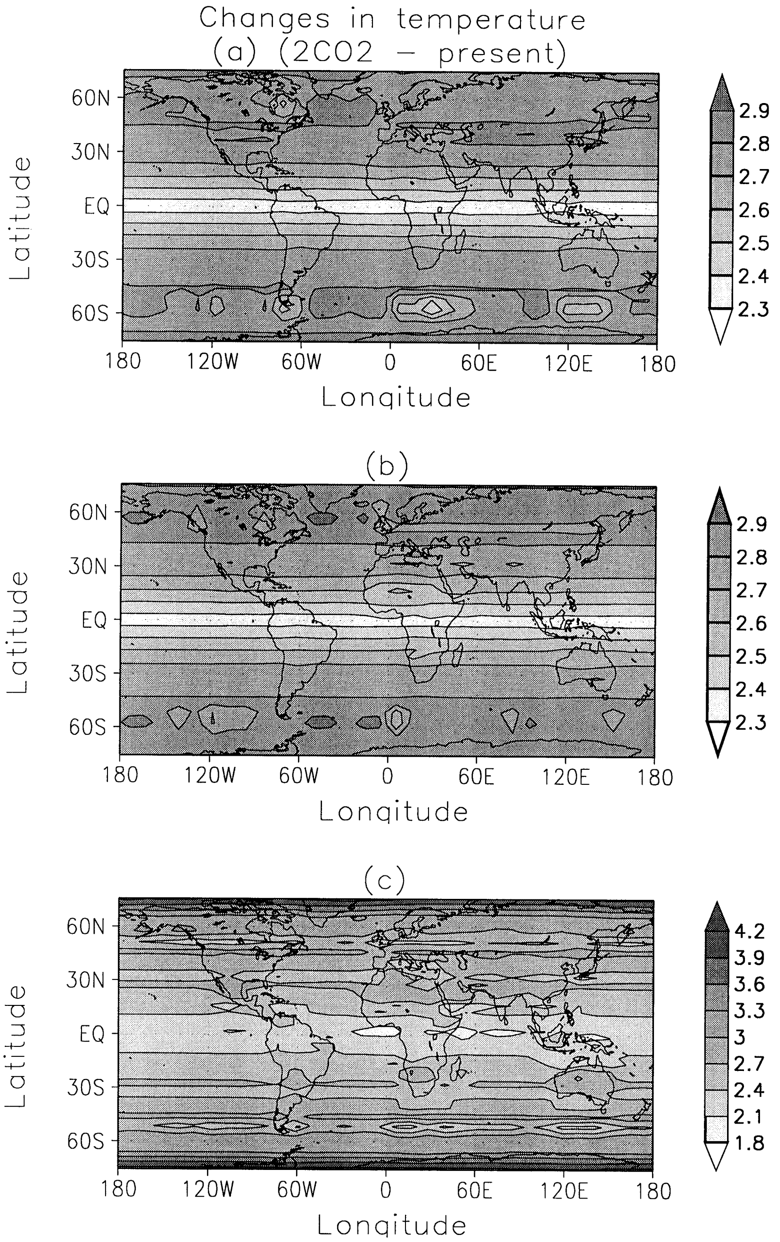

Fig. 5. Changes in temperature (°C) for the present–$2CO_2$ case by (a) maximizing σ_p, (b) maximizing σ_m and (c) maximizing σ_t.

shows important latitudinal changes (Fig. 6c). In this case, the cloud-cover in desert regions does not decrease as much as in other areas (e.g., the Mediterranean basin). Moreover, the cloud-cover increases at the southern pole.

4.2. *Fixed cloud-cover*

In this case, the surface temperature has been obtained by applying extremal principles related to material, total and advective entropy production without using the convective hypothesis (i.e.,

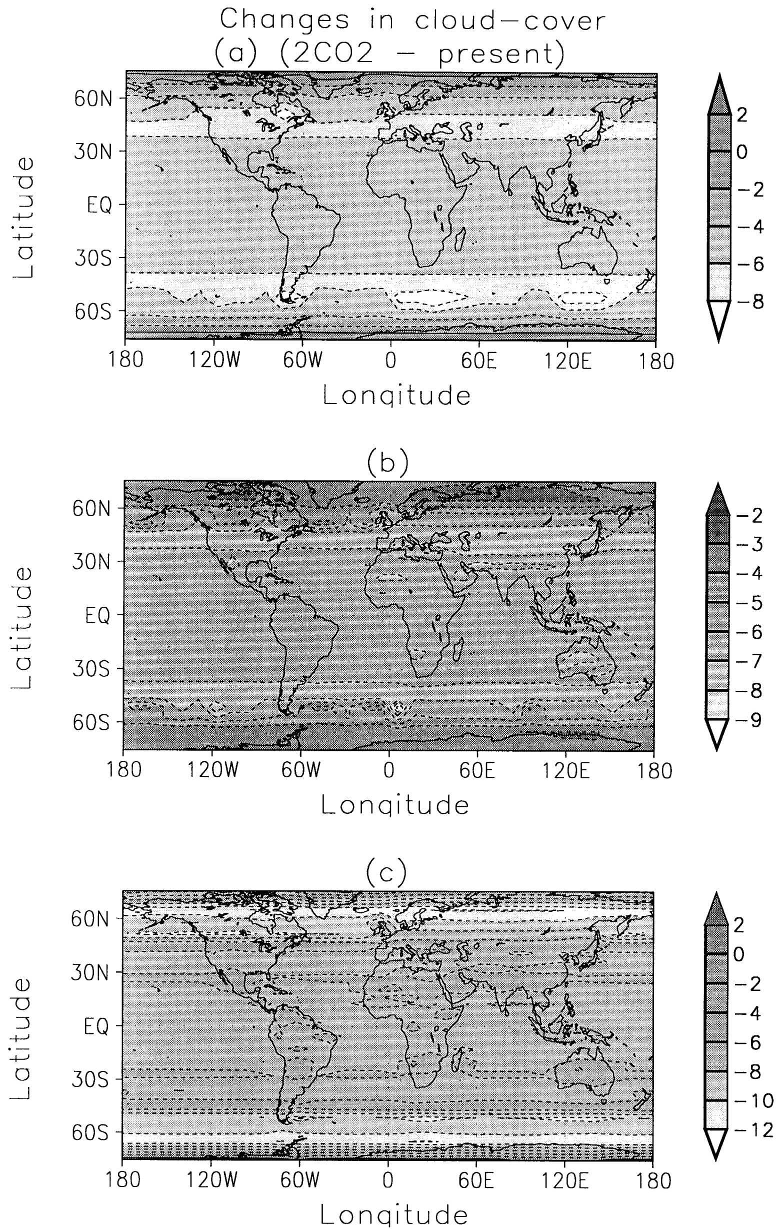

Fig. 6. Changes in cloud-cover (%) for the present–2CO_2 case by (a) maximizing σ_p, (b) maximizing σ_m and (c) maximizing σ_t.

principle of maximum convection). Changes in long-wave parameters for simulating different levels of greenhouse gases are those described in Subsection 4.1. Furthermore, since the cloud-cover has been fixed, only changes in surface albedo produced by the ice-albedo feedback, can vary the planetary albedo and, then, the net balance at TOA. Therefore, globally-averaged changes in long-wave radiation at TOA as well as in planetary albedo do not coincide with those obtained in Subsection 4.1, since they are smaller.

4.2.1. Globally-averaged results. In Table 5, globally-averaged changes of surface temperature T, long-wave radiation at TOA H_{LT} and planetary albedo α_p are shown for different values of CO_2 concentration. The warming at $2CO_2$ for the three different expressions extremized reaches $\approx 1.4°C$, which is nearly a half of that obtained for a variable cloud model. A similar rate of reduction has been found by Manabe and Broccoli (1985) who use a GCM with fixed and variable cloud-cover. In that study, however, the warming in conditions of $2CO_2$ became 2.3°C and 4.0°C respectively. The low-sensitivity of the model to changes in greenhouse gases when the cloud-cover has been fixed, can be observed from the warming of the $4CO_2$ case, which is only 2.8°C.

4.2.2. Zonally-averaged results. Zonally-averaged changes in temperature for the present–$2CO_2$ case are shown in Fig. 7. In this case, the results obtained by maximizing the three rates of entropy production behave similarly. Thus, the warming projected for the three expressions at low latitudes is $\approx 1.1°C$, increasing towards the poles. However, at both pole-boxes the simulations at the maximum states in σ_m or in σ_p give a warming less intense than that obtained at the sub-polar boxes (i.e., boxes ranging from 61.0° to 69.6° degrees of latitude). The sub-polar boxes, equal to the polar-boxes, are regions highly influenced by the reduction of surface albedo due to the increase in surface temperatures.

Table 5. *Globally-averaged changes in T temperature, LE + H latent plus sensible heat fluxes, H_{LT} long-wave radiation fluxes at the top of the atmosphere and α_p planetary albedo for different levels of CO_2; case with ice-albedo feedback and with fixed cloud-cover*

Case ($\times CO_2$)	ΔT (°C)	ΔH_{LT} ($W\,m^{-2}$)	$\Delta\alpha_p$ ($\times 100$)
	maximizing σ_p		
0.5	−1.40	−0.15	0.09
1.5	0.84	0.09	−0.06
2	1.44	0.16	−0.10
3	2.30	0.25	−0.15
4	2.92	0.34	−0.20
	maximizing σ_m		
0.5	−1.37	−0.13	0.07
1.5	0.82	0.08	−0.04
2	1.40	0.13	−0.07
3	2.24	0.22	−0.12
4	2.83	0.25	−0.14
	maximizing σ_t		
0.5	−1.41	−0.16	0.10
1.5	0.84	0.09	−0.06
2	1.44	0.16	−0.10
3	2.30	0.26	−0.15
4	2.91	0.32	−0.19

4.2.3. Horizontal distribution. Changes in temperature vary more with longitude than those obtained with a variable cloud-cover. In Fig. 8a, the 2-Dim horizontal distribution of changes in surface temperature for the present–$2CO_2$ period, through maximizing the advective entropy production σ_p, has been shown. Changes in temperature reach their maximum values at high latitudes. Also, notable warmings have been obtained in desert zones. The equatorial regions over oceans become those zones with the smallest changes in temperature, where the surface temperature does not increase beyond 1.15°C. For the same period, a similar pattern has been obtained by maximizing the rate of material entropy pro-

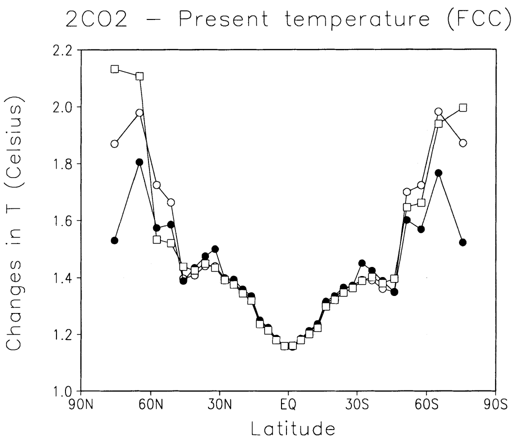

Fig. 7. Zonally-averaged changes in temperature for the present–$2CO_2$ case. Simulations with fixed cloud-cover. Open circle = maximum state in σ_p, closed circle = maximum state in σ_m and open square = maximum state in σ_t.

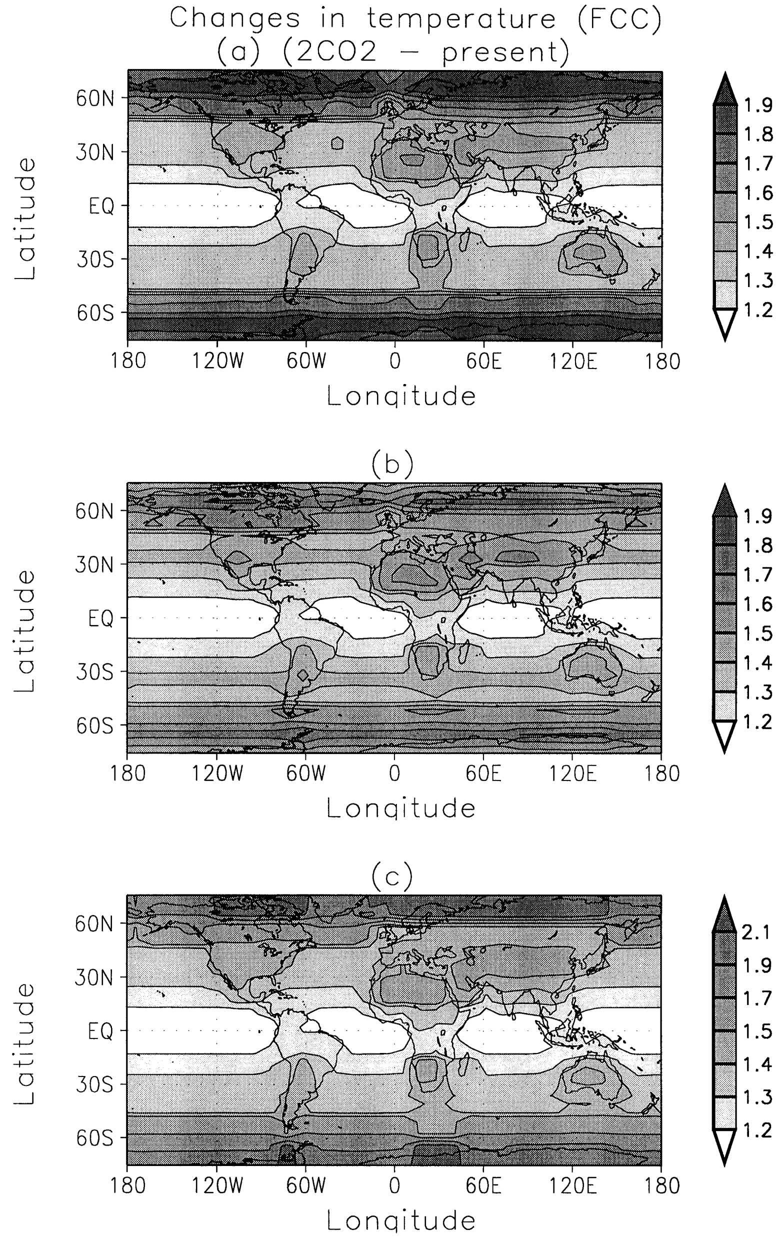

Fig. 8. Changes in temperature (°C) for the present–$2CO_2$ case by (a) maximizing σ_p, (b) maximizing σ_m and (c) maximizing σ_t. Simulations with fixed cloud-cover.

duction σ_m (Fig. 8b). Finally, Fig. 8c shows the increase in surface temperature when the hypothesis of maximum rate of total entropy production σ_t has been used for simulating the present–$2CO_2$ period. In this case, the temperature increases more than 2.1°C at high latitudes. In comparison, the warming over desert zones reaches 1.7°C.

5. Feedback parameters

In Sections 3 and 4, different climatic scenarios for both variable and fixed cloud models have been obtained with and without the ice-albedo feedback. In this section, we quantify the effect of this feedback for a system constrained to follow both maximum convection and dissipation principles or only the extremum dissipation principle.

The effect of the feedback can be quantified by the feedback factor f_T (Schlesinger, 1985)

$$f_T = 1 - \frac{\Delta T_0}{\Delta T}, \tag{1}$$

where ΔT and ΔT_0 are changes in surface temperature with and without the effect of the feedback respectively.

On the other hand, the effect of the feedback to changes in cloud-cover can be represented by means of f_ϑ, defined as

$$f_\vartheta = 1 - \frac{\Delta\vartheta_0}{\Delta\vartheta}, \tag{2}$$

where, as in (1), $\Delta\vartheta$ and $\Delta\vartheta_0$ are changes in cloud fraction with and without the effect of the feedback respectively.

5.1. *Variable cloud model*

In this case, the cloud-cover has been obtained through maximizing both convection and dissipation. This last hypothesis has been applied to the rate of material, advective and total entropy production. In all the cases, $f_T \approx 0.003$ taking the variations corresponding to the present–$2CO_2$ simulation. In comparison, the surface albedo feedback f_T for a two-layer RCM ranges between 0.14 and 0.19 (Schlesinger, 1985). The feedback factor f_ϑ is negative (≈ -0.10 at $2CO_2$ doubling point) and, in fact, greater in magnitude than that due to f_T.

5.2. *Fixed cloud model*

Here, the convective hypothesis has not been applied, since the cloud-cover has been fixed for any scenario. In this case, the feedback factor for the different cases f_T is ≈ 0.07, and greater to that obtained for a variable cloud model.

6. Conclusions

In this paper, different climatic scenarios have been analyzed by using a simple 2-Dim horizontal EBM subject to a global constraint for dissipation (i.e., entropy production) and convection. The application of an extremal principle to the climatic system is based on the thermodynamics theory, the rate of entropy production being a feasible variable for this type of behaviour. Due to both maximum convection and dissipation hypotheses have not been fully demonstrated, the predictive capability of both hypotheses has been extensively analyzed. Thus similarities with real data and usual simulations can provide an additional support for the application of such principles.

Extremal climatic simulations carried out in the 2-Dim model consider the cloud-cover either predicted by the hypothesis of maximum convection or kept fixed. The variable cloud model produces a globally-averaged warming from pre-industrial conditions ≈ 0.9°C, assuming both direct and indirect (moderate) effects of aerosols. For the same period the model simulates a decrease in cloud fraction ≈ 0.5% for the maximum state in material dissipation, or an increase $\approx$ 0.2% for the maximum state in total entropy production. By using the same conditions for the pre-industrial–present period, the warming produced by the fixed cloud model reaches ≈ 0.2°C. The small change in temperature simulated for the fixed cloud model has been also obtained for possible future scenarios. Thus, for example, the variable cloud model obtains a globally-averaged warming ≈ 2.7°C for the present–$2CO_2$ period (assuming an equivalent radiative forcing at TOA $\approx$ 4.4 W m^{-2}), with a reduction in cloud fraction between 5.4% and 4.4% depending on the expression maximized. The same model but with fixed clouds, generates a globally-averaged warming ≈ 1.4°C.

Moreover, zonally-averaged results for different hypotheses differ considerably. The latitudinal distribution of changes in temperature at the maximum state in total entropy production becomes less homogeneous than simulations obtained through maximizing both material and advective rates of entropy production. Also, different distributions of changes in cloud-cover have been obtained. Thus, for example, if the greenhouse gases increase, the maximum state in the advective rate of entropy production predicts a maximum warming at the poles with an increase in cloud-cover for these regions. In contrast, the climate at the maximum rate of material entropy production simulates a decrease in cloud-cover at the poles.

In Part I, we found that the hypothesis of maximum in σ_m could properly simulate the current climate, since the results obtained with and without fixed cloud-cover generate a similar climatic distribution, being reasonable by taking the intrinsic limitations of the model used. In contrast, the current climate at the maximum state in σ_t was found to depend on the convective hypothesis.

On the other hand, although the effect of a variable cloud-cover could be nearly irrelevant for the climate obtained at current conditions (see the case maximum in σ_m in Part I), it is of utmost importance in order to elucidate the climate in other scenarios. Furthermore, if the real climate is only governed by an extremal principle in dissipation but not in convection, and the variation in cloud-cover is unknown, the results with and without fixed cloud-cover would represent the possible range of variation for the main climatic variables. In fact, if we assume that the current climate is close to the simulated state using both maximum convection and dissipation hypotheses, variations in cloud-cover become maxima when the convective hypothesis is applied and minima when the cloud-cover does not vary. In this case, for example, the real change in temperature for the pre-industrial–present state would be located between 0.2°C and 0.9°C with a possible change in cloud-cover from +0.2% to −0.5% (depending on the dissipation hypothesis). For the present–$2CO_2$ period, the globally-averaged warming predicted by the model constraint to dissipative hypotheses would be between 1.4°C and 2.8°C, with a variation in cloud-cover between 0% and −5.4%. In fact, the role of clouds on simulating a given scenario is an important source of uncertainty, which, for example, means that different models obtain results from 2°C to 5°C at the $2CO_2$ doubling point (Ramstein et al., 1998).

From the above results and in comparison with measured data and values simulated by usual climatic models, the hypothesis of maximum total entropy production σ_t appears to be the most reasonable due to (1) its low sensitivity to changes in cloud-cover, and (2) the high sensitivity at pole boxes. In addition, changes in greenhouse-gases when applying the hypothesis of maximum rate of total entropy production σ_t produce both positive and negative latitudinal variations in cloud-cover, which appear more reasonable than changes of cloud-cover in only one direction for the entire globe (as those obtained by using σ_m). Thus, the hypothesis of maximum rate of total entropy production could be connected with the idea of a universal requirement of entropy increase in the universe (Ozawa and Ohmura, 1997). The unsuccessfully result of applying this principle in 1-Dim diffusive models (Pujol and Llebot, 1999), may be caused by the absence of the convection in these types of models, being impossible to use the hypothesis of maximum convection.

On the other hand, although the hypothesis of maximum rate of material entropy production σ_m produces reasonable results for the current climate (in several climate models; see Part I), its low sensitivity at high latitudes for different climatic scenarios (as simulated by the present 2-D model) is unexpected.

Furthermore, due to the climate is subject to important internal and external changes, we could assume some long-term episodes where the general requirement for the fulfilment of an extremal principle was not achieved. In this case, the climate could vary following different dissipation hypotheses. For example, the climate at current conditions could follow the maximum dissipation principle in σ_t plus the convective hypothesis (or the maximum dissipation principle in σ_m). In contrast, the climate obtained by a fixed cloud model at the maximum state in total entropy production would become similar to that expected in the Mesozoic, where the temperatures at high latitudes were 10°C or more warmer than the present state with a little change at low latitudes (Rind, 1998). However, the mechanisms that would vary the extremal state achieved by the climate, if it really exists, remain unknown.

7. Acknowledgements

This work has been partially supported by the Ministerio de Educación y Cultura of the Spanish Government under contract PB96-0451.

REFERENCES

Charlson, R. J., Schwartz, S. E., Hales, J. M., Cess, R. D., Coakley, Jr. J. A., Hansen, J. E. and Hoffmann, D. J. 1992. Climate forcing by anthropogenic aerosols. *Science* **255**, 423–429.

Grassl, H. 1981. The climate at maximum entropy production by meridional atmospheric and oceanic heat fluxes. *Q. J. R. Meteorol. Soc.* **107**, 153–166.

Haywood, J. M. and Ramaswamy, V. 1998. Global sensitivity studies of the direct radiative forcing due to anthropogenic sulfate and black carbon aerosols. *J. Geophys. Res.* **103**, 6043–6058.

Hewitt, C. D. and Mitchell, J. F. B. 1997. Radiative forcing and response of a GCM to ice age boundary conditions: cloud feedback and climate sensitivity. *Clim. Dyn.* **13**, 821–834.

IPCC: Intergovernmental Panel on Climate Control, 1995. *The science of climate change*, edited by Houghton, J. T., Meira Filho, L. G., Callander, B. A., Harris, N., Kattenberg, A. and Maskell, K. Cambridge Univ. Press, New York.

Kacholia, K. and Reck, R. A. 1997. Comparison of global climate change simulations for $2 \times CO_2$-induced warming. *Clim. Change* **35**, 53–69.

Langner, J., Rodhe, H., Crutzen, P. J. and Zimmermann, P. 1992. Anthropogenic influence on the distribution of tropospheric sulphate aerosols. *Nature* **349**, 712–715.

Manabe, S. and Broccoli, A. J. 1985. A comparison of climate model sensitivity with data from the last glacial maximum. *J. Atmos. Sci.* **42**, 2643–2651.

Mitchell, J. F. B., Johns, T. C., Gregory, J. M. and Tett, S. F. B. 1995. Climate response to increasing levels of greenhouse gases and sulphate aerosols. *Nature* **376**, 501–504.

Ozawa, H. and Ohmura A. 1997. Thermodynamics of a global-mean state of the atmosphere — a state of maximum entropy increase. *J. Climate* **10**, 441–445.

Planck, M. 1913. *Heat radiation* (trans), 2nd edition, republished 1959. Dover, New York.

Pujol, T. and Llebot, J. E. 1999. Second differential of the entropy as a criteria for the stability in low-dimensional climate models. *Q. J. R. Meteorol. Soc.* **125**, 91–106.

Ramstein, G., Serafini-Le Treut, Y., Le Treut, H., Forichon, M. and Joussame, S. 1998. Cloud processes associated with past and future climate changes. *Clim. Dyn.* **14**, 233–247.

Reader, M. C. and Boer, G. J. 1998. The modification of greenhouse gas warming by the direct effect of sulphate aerosols. *Clim. Dyn.* **14**, 593–607.

Rind, D. 1998. Latitudinal temperature gradients and climate changes. *J. Geophys. Res.* **103**, 5943–5971.

Schlesinger, M. E. (editor) 1985. *Physically-based modelling and simulation of climate and climatic change. Part 2.* NATO ASI Series C: Mathematical and Physical Sciences, vol 243. Kluwer A. P. Dordrecht.

Senior, C. A. and Mitchell, J. F. B. 1993. Carbon dioxide and climate: the impact of cloud parameterization. *J. Climate* **6**, 393–418.

Taylor, K. E. and Penner, J. E. 1994. Response of the climate system to atmospheric aerosols and greenhouse gases. *Nature* **369**, 734–737.